Chapter 3

Localizing and Quantifying Carotenoids in Intact Cells and Tissues

Jerilyn A. Timlin, Aaron M. Collins, Thomas A. Beechem, Maria Shumskaya and Eleanore T. Wurtzel

Additional information is available at the end of the chapter

http://dx.doi.org/10.5772/68101

Abstract

Raman spectroscopy provides detailed information about the molecular structure of carotenoids. Advances in detector sensitivity and acquisition speed have driven the expansion of Raman spectroscopy from a bulk analytical tool to a powerful method for mapping carotenoid abundance in cells and tissues. In many applications, the technique is compatible with living organisms, providing highly specific molecular structure information in intact cells and tissues with subcellular spatial resolution. This leads to spatial-temporal-chemical resolution critical to understanding the complex processes in the life cycle of carotenoids and other biomolecules.

Keywords: vibrational spectroscopy, multivariate analysis, confocal Raman microscopy, Raman imaging, photosynthetic organisms, carotenoids, resonance Raman scattering

1. Introduction

Carotenoids are tetraterpenoids and have various functions in plants and algae. They extend the range of wavelengths for photosynthesis by harnessing solar radiation where chlorophyll pigments do not appreciably absorb and serve as structural elements within the photosynthetic apparatus [1]. They also function to dissipate excess solar radiation and prevent the formation of harmful singlet oxygen species [2]. Additionally, in specific photosynthetic eukaryotes, carotenoids accumulate in plastid organelles called chromoplasts and give many fruits, flowers, and roots their bright colors [3]. For these reasons, assessing the presence and distribution of carotenoids at the subcellular level provides a keyhole through which to

understand a variety of cellular processes. The use and utility of Raman imaging is addressed here toward this end.

The Raman effect involves an incoming photon being scattered inelastically by a polyatomic molecule. This phenomenon requires that energy is exchanged between the photon and molecule. Since energy levels in the molecule are discrete, the difference in energy between the incoming and scattered photon corresponds to a molecular transition, most typically a vibration [4]. Molecular vibrations are influenced by the composition of atoms that make up the molecule, the types of bonds that connect atoms, and molecular symmetry. Thus, Raman spectroscopy has been exploited as a highly sensitive analytical tool for the determination of the chemical identity of many molecules [5, 6]. The probability of observing the Raman effect is low, however, as the intensity of scattered radiation scales with the fourth power of incident light's frequency. The Raman effect is oftentimes considerably weaker as compared to the intrinsic fluorescence in cells and tissues, complicating and even prohibiting the detection of the Raman scatter in biologically relevant matrices.

However, if the frequency of incident light matches the energy of an electronic transition, an enhancement of the Raman signal may be observed. This is known as resonance Raman scattering (RRS), which can enhance the signal by several orders of magnitude over a "normal," nonresonance measurement. In fact, the resonance effect can increase the scattering cross section to exceed any off-resonance Raman scatter and, importantly, even rival intrinsic fluorescence from the species. RRS thus has profound analytical potential and has been comprehensively reviewed elsewhere for the general life science field [7] and specifically for applications in photosynthesis [8]. Here, its role in the assessment of carotenoids is examined explicitly.

The optical properties of carotenoids make them especially suitable for RRS. Carotenoids are π-electron-conjugated carbon-chain molecules consisting of alternating C—C single bonds and C═C double bonds. Individual carotenoids can be distinguished by the number of conjugated carbon double bonds, the number of attached methyl side groups, and the number and type of end groups. These properties result in many of the highly abundant carotenoid molecules (e.g., β-carotene, zeaxanthin, lycopene, and lutein) having distinct, yet broad (100 nm) absorption bands in the visible region of the spectrum. The absorption shifts to longer wavelengths as the effective conjugation length of the carotenoid increases. Fortuitously, these visible absorption bands overlap with the common laser wavelengths for Raman excitation. Thus, when excited under these conditions, carotenoids exhibit a very strong RRS response (enhancement factor of about five orders of magnitude relative to non-resonant Raman spectroscopy) and little to no fluorescence emission. Additionally, variations in absorption of the different carotenoids can be exploited by shifting the excitation wavelength (a technique also known as "tuning") to preferentially excite different carotenoid molecules. Owing to these amenities, RRS therefore enables the detection of carotenoids, even in complex biological systems, such as living photosynthetic cells and tissues.

The majority of carotenoids have linear structures resulting in a limited number of Raman-observable vibrations that are easily categorized into a distinct vibrational signature. There are three major Raman modes typically leveraged in the analysis of carotenoids [9, 10]. The ν_1 band (~1530 cm^{-1}) arises from the stretching vibrations of the conjugated C═C backbone. This band is sensitive to conjugation length and molecular conformation and therefore

http://dx.doi.org/10.5772/68101

is the most diagnostic for carotenoid identity. The ν_2 band (~1160 cm^{-1}) emerges from the stretching of the C—C vibrations coupled to C—CH_3 stretches or C—H in-plane bending. The ν_3 band (~1006 cm^{-1}) is attributed to CH_3 in-plane–rocking modes. Importantly, the vibrational modes are more or less insensitive to the molecular environment [11] meaning that a carotenoid found within the tissues of a plant may have a very similar spectrum to the same carotenoid dissolved in solvent. This observation is important when assigning carotenoid signatures *in situ*. **Figure 1** shows the resonance Raman spectra from six common carotenoids produced in photosynthetic organisms. The spectra are plotted in the order of increasing

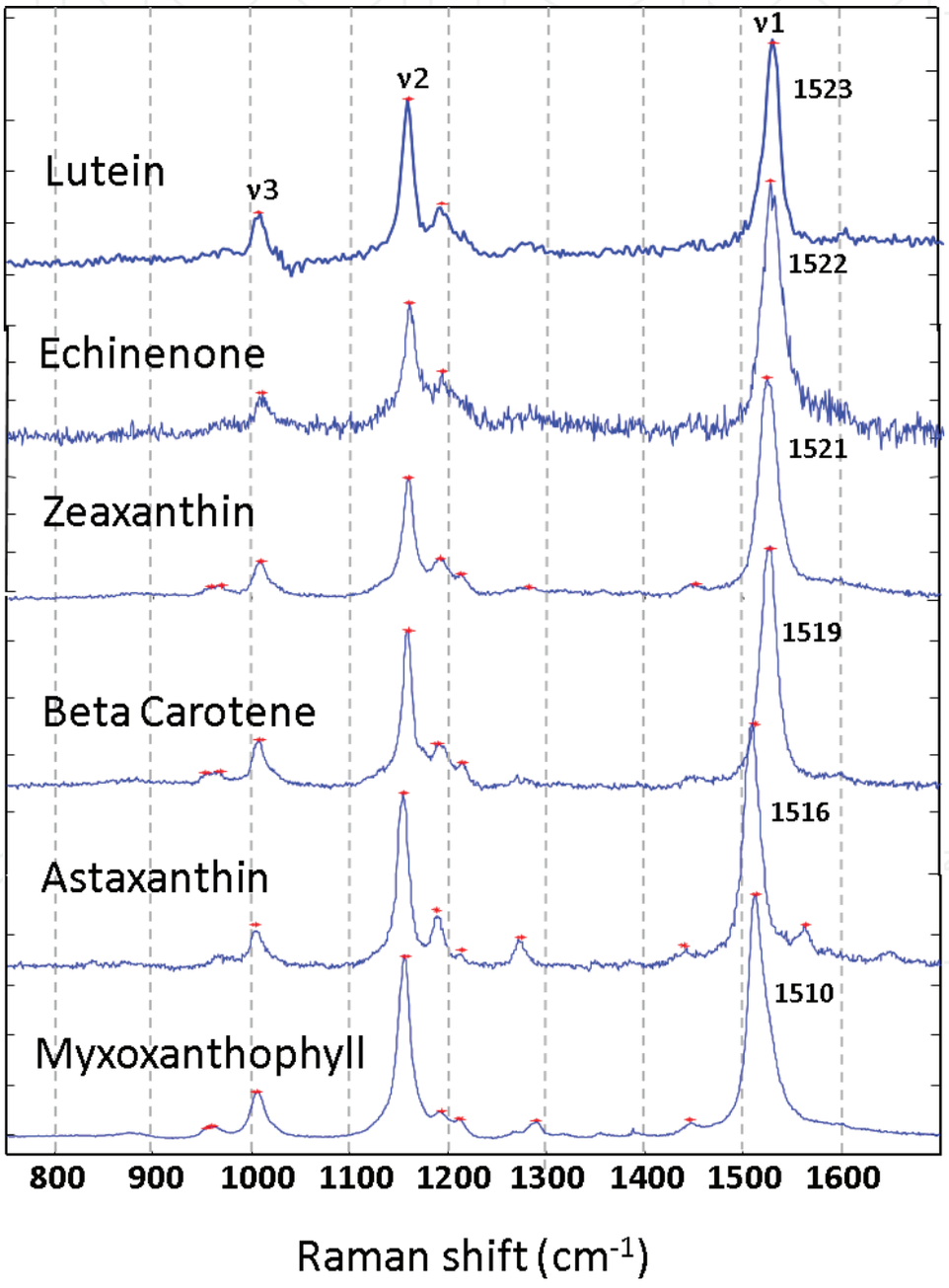

Figure 1. Resonance Raman spectra of six common carotenoids produced in photosynthetic organisms. Major Raman active vibrations are labeled. Spectra were obtained from carotenoids in powder form with the exception of lutein which was dissolved in methanol.

ν_1 vibration position (ranging from 1516 to 1524 cm^{-1}) and illustrate the ability to distinguish carotenoids by the position of this vibration.

In recent years, advances in detector sensitivity and acquisition speed have driven the expansion of Raman spectroscopy from a bulk analytical tool to a powerful method for mapping molecular vibrations in cells and tissues by the addition of a spatial dimension. Spatial resolution available with Raman microscopy is dependent on the wavelength of the excitation light and in theory is the same as other optical microscopies, such as fluorescence (e.g., ~250 nm lateral and ~500 nm axial, for blue/green excitation). The addition of spatial resolution can be accomplished in several different ways: confocal point-scanning Raman microscopy [12, 13], wide-field Raman imaging [14], or Raman line scanning [15, 16]. The relative advantages and disadvantages of each of these approaches have been reviewed elsewhere and will not be covered here [17]. In addition to the imaging methodology, spectral information can be obtained from either a single or a small number of bands through the use of discrete bandpass filters or tunable filters or in a hyperspectral fashion, where the entire Raman spectrum is dispersed via a prism or grating allowing for the simultaneous acquisition of hundreds of spectral bands. While there is typically a speed advantage associated with the filter-based acquisition approach, recent commercial systems utilizing electron-multiplied charge-coupled device (EM-CCD) detectors and cutting-edge research systems [18] are able to approach confocal fluorescence microscopy speeds and further improvements are expected.

Given the complexity associated with biological matrices such as live cells and tissues, hyperspectral Raman approaches are often advantageous because they can provide detailed spectral signatures for subsequent analysis of weak or overlapping features and background noise reduction using chemometric algorithms. These approaches are collectively referred in the literature as Raman spectroscopic imaging, or hyperspectral Raman microscopy. Additionally, confocal point scanning or pseudo-confocal line scanning can have advantages due to the inherent rejection of out-of-focus signal provided by the pinhole or entrance slit, respectively. A confocal, point-scanning, hyperspectral Raman microscope was utilized for the work presented in this chapter as it adequately rejects the intense pigment signal from outside the focal plane, while providing reasonable acquisition speeds for live cells.

Recent literature shows that Raman spectroscopic imaging is emerging as a key technology for single-cell analysis, including *in vivo* lipidomics [19], chemical composition of bacterial cells [20], lignin in plant cell walls [21], and metabolism in combination with stable isotope incorporation [22–24]. Researchers have also begun capitalizing on the specific benefits of resonance Raman spectroscopic imaging to localize carotenoids in individual cells and tissues. Pudney et al. demonstrated the localization of lutein, beta-carotene, and lycopene in several tomato varieties [25]. Zheng and coworkers used Raman imaging to investigate biofilm formation in Rhodococcus sp. SD-74, showing that biofilm production by this organism is correlated with increasing carotenoid concentrations, a finding not possible with traditional dye staining assays or electron microscopy [26]. Kilcrease et al. utilized a novel combination of confocal Raman microscopy with laser scanning confocal and scanning and transmission electron microscopy to demonstrate subcellular accumulation sites of various carotenoids in *Capsicum annuum* L. (Chile pepper) fruit. Their work discovered an unexpected relationship between carotenoid accumulation and chromoplast structure. Collins and coworkers utilized hyperspectral confocal Raman microscopy to study fundamental carotenoid biogenesis in *Haematococcus pluvialis*

throughout the organism's life cycle [27]. Additionally, although not single cell work, Toomey et al. recently show the utility of hyperspectral confocal Raman microscopy for investigating carotenoid composition in single oil droplets within the avian retina [28].

While Raman spectroscopic imaging has potential for assessing carotenoid distributions in single cells and tissues for many applications in biomedicine and photosynthesis, there are some noteworthy limitations. First, not all carotenoids are enhanced to the same degree and some will not be enhanced at all. This differential enhancement can be advantageous, but it also can pose limitations for certain carotenoids. To some degree, the choice of laser excitation can target additional carotenoids. However, performing multiple Raman microscopy scans at two or more excitation wavelengths is prohibitive for live-cell dynamics and may require fixed samples depending on the acquisition times. Second, even with high spectral resolution instruments, multiple carotenoid species with highly overlapping, similar peaks can be difficult to identify. Additionally, even with resonance enhancement, Raman peaks may still be weak at *in vivo* and *in planta* relevant concentrations and be overwhelmed by background fluorescence depending on the sample matrix.

In addition to the hardware approaches listed above, the first two limitations are actively being addressed with the development of robust multivariate analysis tools [29–31]. For example, multivariate curve resolution (MCR) has been developed by several research groups for the analysis of hyperspectral confocal fluorescence and Raman image data sets [29, 32–34] finding success in complex multicomponent biological samples. It is therefore used in the analysis presented in this chapter. Lastly, while recent advances in fluorescence microscopy have extended the spatial resolution beyond the diffraction limit, the spatial resolution of Raman spectroscopic imaging is still in many cases orders of magnitude larger than the biological processes being investigated. Near-field approaches can provide higher spatial resolution, but have not found wide-scale success with living cells and tissues [35].

This chapter presents three separate applications of confocal Raman microscopy to assess carotenoid localization and relative abundance within living cells. The green algae *H. pluvialis* is presented to highlight the ability to discern highly similar carotenoid structures in algal cells. Maize (*Zea mays*) protoplasts demonstrate the localization of carotenoids even amidst a high background of chlorophyll pigment. Finally, *Synechocystis* sp. PCC6803, a model cyanobacterium, is presented to illustrate carotenoid localization even in very small microbes. Together, these applications demonstrate the potential of resonance Raman microscopy and imaging for the analysis of carotenoid localization and abundance at the single-cell and subcellular levels in photosynthetic organisms.

2. Materials and methods

2.1. Cell culture and sample prep

H. pluvialis cells were obtained from the Hu lab cultured as described previously to produce cultures at various stages of the life cycle (flagellated, nonmotile palmelloid, and aplanospores) [27]. Cells suspended in growth media were directly loaded to a slide and covered with a glass coverslip. In this arrangement, cells remained hydrated during the duration of the imaging.

Synechocystis 6803 cells were obtained from the Pakrasi lab and cultured in BG-11 media (UTEX recipe) in baffled flasks in a temperature-controlled incubator under continuous light (~30 μmol m^{-2} s^{-1}, cool white fluorescent lights) with shaking (60 rpm). Prior to imaging, a 4-μl sample was directly pipetted onto a BG-11 agar-coated slide and covered with a glass coverslip. Cells were immediately imaged.

Etiolated maize protoplasts were isolated from *Z. mays* var. B73 leaves as described previously [36]. Released protoplasts were collected, washed, and shipped in a buffer solution overnight for Raman imaging. Upon arrival, protoplasts were concentrated by centrifugation at 500 × g and removal of all but 100 μl of the supernatant. Concentrated sample (25 μl) was loaded into an *in situ* frame (Gene Frame, ThermoFisher) previously adhered to a gridded microscope slide (Lovins Micro-Slide Field Finder, Electron Microscopy Sciences) and covered with a glass coverslip. The gridded slide was used to perform correlated fluorescence microscopy for a separate experiment. Protoplasts were immediately imaged.

2.2. Confocal Raman microscopy

Raman images were acquired with a WiTec Alpha300R system equipped with a WiTec UHTS spectrometer utilizing a 600-l/mm grating and an Andor back-illuminated electron-multiplying charge-coupled device (EMCCD). Light was incident at 532 nm and focused using a 50×/0.55 NA objective (*Synechocystis* 6803), 20×/0.45 NA objective (maize protoplasts), and a 100×/0.9 NA objective (*H. pluvialis*). Laser powers were chosen such that the spectral character was nearly invariant with time and did not cause a visible change in the sample during collection. In most cases, power incident on the surface was held to less than 1 mW. The acquisition time per spectrum was chosen to provide adequate signal to noise to perform the multivariate analysis and varied for the different samples analyzed ranging from 4 to 10 ms per spectrum. The spectral response was 3 cm^{-1} per pixel, which through fitting resulted in the ability to specify peak position to an absolute accuracy of ±1 cm^{-1}. All measurements were performed in an unpolarized back-scattering arrangement. Images were acquired by scanning the sample using a piezo-stage possessing a lateral resolution of <5 nm. Raman-scattered light is collected continuously across the sample such that every spectrum is the average convolution of the beam intensity and sample response over the distance defining an individual voxel. Images were collected by acquiring a spectrum every 333 nm (*Synechocystis* 6803 and *H. pluvialis*) or 500 nm (maize protoplasts). Raman shifts were calibrated using the well-established positions of silicon, 6H-SiC, graphite, and 4-acetameniphol.

2.3. Image data analysis

All spectral image analysis was performed in Matlab 2012 or 2015 (Mathworks) equipped with the statistics and machine learning, signal processing, image processing, and curve fitting toolboxes leveraging in-house written software, functions, and scripts. Hyperspectral confocal Raman images were preprocessed to remove cosmic spikes [37]. When applicable, images from the same sample were compiled into a composite image data set. The use of composite images, rather than analyzing every image independently, increases the number of pixels for the MCR analysis and thus serves to improve spectral signature identification by adding additional variance [38]. The spectral region was trimmed to exclude the excitation

laser line but still include about 5–10 pixels of the spectrum where the signal was blocked by the Rayleigh filter. This technique assists in the analysis by providing a "zero-signal region" for assessing baseline contributions and is discussed in detail by Jones et al. [38]. In most cases, an image mask was created that excluded pixels outside the area of the cells from the analysis as they contain predominantly background signal.

Principal components analysis (PCA) was performed on the composite image and the Scree plot was inspected to determine the number of independent components present in the image data set (measured as being before the bend in the elbow of the Scree plot [29]). Multivariate curve resolution was then performed using a constrained alternating least-squares algorithm and employing robust constraints for equality (offset/baseline) and non-negativity (all true spectral components) to develop a spectral model that described the spectral variance within the data set. A PCA analysis of the residuals was used to confirm the appropriateness of the spectral model for describing the data and identify any unmodeled spectral signatures. The multivariate curve resolution algorithm [39–43] and specific approaches for success with biological images have been described in detail elsewhere [29, 38]. The details of the spectral models developed are presented during the results and discussion for each application in this chapter. The MCR-identified spectra were then used in a classical least-squares (CLS) analysis to predict the concentrations of each spectral component in each image pixel. Lastly, the resulting concentration maps were exported as 16-bit grayscale tiffs such that they could be subject to traditional image analysis. Color image overlays and simple image cropping and scaling for visualization purposes was performed in Fiji [44].

3. Results and discussion

3.1. Resolving different carotenoids in living cells: *H. pluvialis*

H. pluvialis is a freshwater green microalga that can synthesize and accumulate astaxanthin, a high-value nutraceutical, under stress conditions such as nutrient deprivation. Though some aspects of carotenogenesis leading to astaxanthin production are well understood, spatial-temporal details of key carotenoids and enzymes have yet to be fully elucidated. In previous work, Collins and coworkers used confocal Raman spectroscopic imaging to provide *in vivo* resolution and localization of beta-carotene and astaxanthin, along with chlorophyll throughout the life cycle of *H. pluvialis* cells [27]. While this work will not be reproduced in detail, here, some key elements will be presented to illustrate the potential of the technique for carotenoids localization in living cells. **Figure 2** demonstrates the advantage of performing MCR analysis on the Raman spectroscopic image data as compared to simplistic band integration. While the image produced by integrating the area under the ν_1 carotenoid vibration provides a highly resolved view of carotenoid location within the cell, the image is a superposition of two different carotenoids found in the cell. By contrast, MCR analysis resulted in a four-component model consisting of two carotenoid spectra (astaxanthin and beta-carotene), chlorophyll, and an autofluorescence component. (Note: A background component was also part of the model, but is omitted here for simplic-

ity.) MCR analysis also generates a corresponding concentration map (i.e., image) for each of these species. This results in an exquisite degree of chemical resolution that allows for quantitative assessment via traditional image analysis methods. In **Figure 2D**, the images for astaxanthin, beta-carotene, and chlorophyll are pseudocolored and overlaid for qualitative comparison. Importantly, in this example, the MCR analysis reveals that astaxanthin is located only in the cytosol. Beta-carotene, meanwhile, is both co-located with astaxanthin in the cytosol, as well as with the chlorophyll in the chloroplast. Together, these Raman images provide spatial-temporal details of astaxanthin production and accumulation in this organism.

3.2. Carotenoids in high-chlorophyll backgrounds: maize protoplasts

Similar to algae, plant carotenoids have roles in light harvesting and protection against light and heat stress. Metabolic engineering of carotenoids in plants has the potential to create varieties exhibiting increased adaptation to climate change as well as additional nutritional value. To develop plant cultivars with these enhanced properties, it is critical to understand the detailed spatial-temporal arrangement of both carotenoids and chlorophyll *in situ*. While chlorophyll is straightforward to detect with a standard confocal fluorescence microscope, carotenoids have little to no detectable fluorescence signal and are not amenable to exogenous labeling.

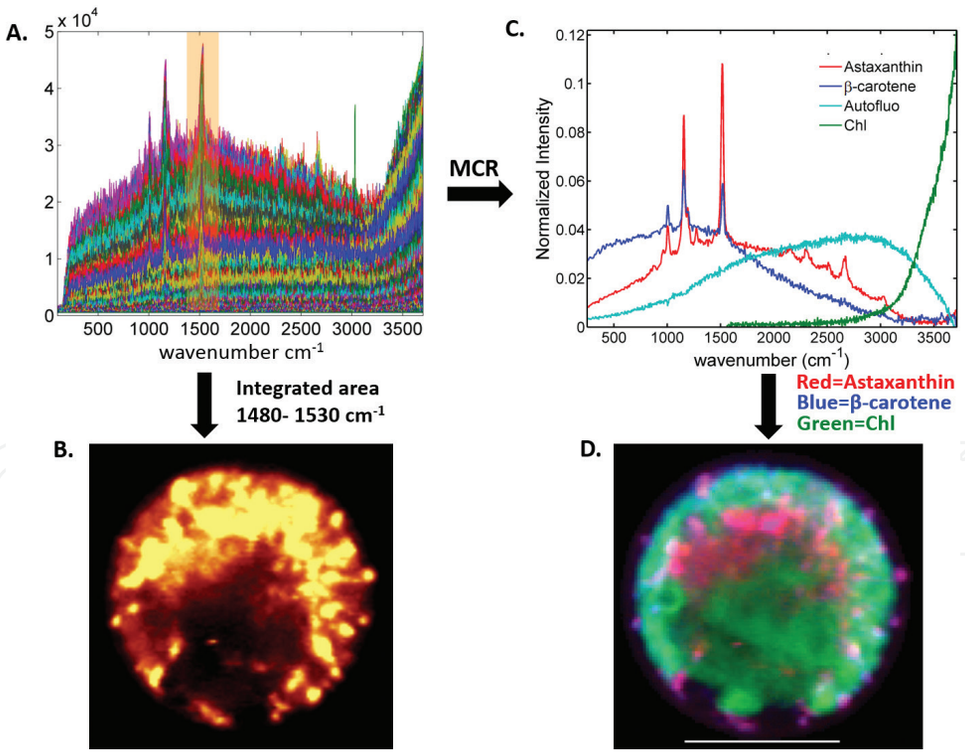

Figure 2. Raman-spectroscopic imaging of *H. pluvialis*: the advantage of MCR analysis. (A) Raw spectra from Raman-spectroscopic image of *H. pluvialis*. (B) Integrated Raman image created by traditional integration over the area of the ν_1 band of the carotenoid (1480–1530 cm^{-1}) for the image data in A. C. MCR identified spectral component from image data in A. RGB image created by overlaying the independent component maps generated in the MCR analysis. Scale bar = *10 μm*. (note: **Figure 2** is best viewed in color. Please refer to the online version of this chapter for the color version of **Figure 2**).

http://dx.doi.org/10.5772/68101

Confocal Raman spectroscopic imaging is capable of detecting carotenoids without the use of any exogenous labels and does so by detecting the resonance Raman signal of carotenoids. This signal can be observed also within the background of other pigments, such as the chlorophyll precursor, protochlorophyllide, which is found in cells of etiolated tissue [45] such as plant protoplasts from etiolated maize (**Figure 3**). Plant protoplasts are plant cells that have their cell wall removed through enzyme treatment and thus are an excellent experimental system for plant biologists because they improve the ease of introducing new genes.

Figure 3 highlights the spatial location and levels of carotenoids and protochlorophyllide in plastids (immature chloroplasts) of etiolated maize protoplasts as observed by confocal Raman microscopy. Previous high-performance liquid chromatography data have shown that the dominant carotenoid in maize-etiolated protoplasts is lutein with a minor amount of violaxanthin (data not shown). The peak positions (ν_1 = 1525 cm^{-1} and ν_2 = 1157 cm^{-1}) in the isolated Raman spectrum shown in **Figure 3C** are consistent with the purified lutein spectrum in **Figure 1** and by Collins et al. [27]. The slight deviation is likely a result of the violaxanthin contribution as the ν_1 vibration of violaxanthin is typically 1528–1530 cm^{-1} [46]. For comparison, Panels A and B show the correlated bright-field and confocal fluorescence chlorophyll images, respectively, for the cell shown in **Figure 3D**. Individual component images are shown in grayscale as well as the red-green merged image (please refer to the online version for color figure). Green corresponds to the carotenoid and red corresponds to the protochlorophyllide pigments in these figures. Localization is confined to the plastids (bright foci ~1 μm in size within the protoplast). Interestingly, a high degree of variation in carotenoid and chlorophyll composition within individual plastids is observed. An example of this heterogeneity is indicated by the yellow arrows in the merged image of **Figure 3D**. These arrows highlight plastids that have predominantly carotenoid (green), predominantly protochlorophyllide (red), or roughly equal amounts of both (yellowish-orange). These differences in relative abundance could arise from differences in the developmental phase or carotenoid abundance. The observed heterogeneities raise important scientific questions about carotenoid biogenesis that Raman-spectroscopic imaging is well poised to answer in future research.

3.3. Approaching the limits of spatial resolution: *Synechocystis* 6803

Cyanobacteria and closely related organisms are thought to be the evolutionary ancestors to chloroplasts found in plants. Cyanobacteria perform photosynthesis to convert light energy to chemical energy and play key roles in the ecology of the earth. Light is harvested by photosynthetic antennae, which are pigment-protein complexes composed of pigments with varying absorption and emission properties in order to "funnel" the energy to the reaction center where it is converted to chemical energy [47]. Carotenoids are integrated into the membrane-associated photosynthetic antennae complexes as well as the photosystems of all cyanobacteria and fundamentally coupled to the processes of light harvesting and photosynthesis. Unfortunately, carotenoids in cyanobacteria are often quite difficult to localize *in situ* because of the very small size of many of the cyanobacteria (1.5–4 μm for the most species) and the co-localization in complexes with highly fluorescent light-harvesting pigments, like phycobilins and chlorophylls. Previous work with hyperspectral confocal fluorescence microscopy has demonstrated sensitivity for localization carotenoids via resonance Raman signatures in

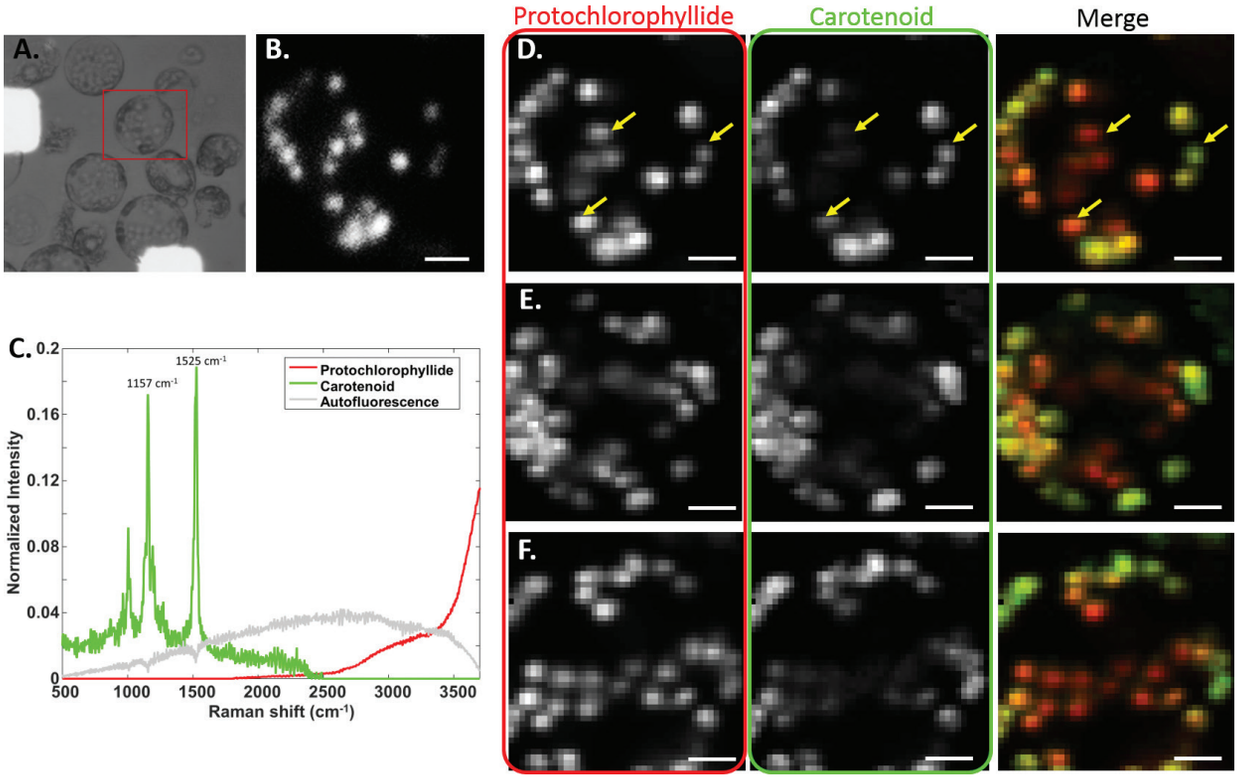

Figure 3. Confocal Raman-spectroscopic imaging of carotenoids and protochlorophyllide in etiolated maize protoplasts. (A) Bright-field image of several protoplasts with red square highlighting single protoplast imaged in B and D. (B) Confocal fluorescence image of cell highlighted in A (chlorophyll emission channel). (C) Spectral components of MCR model from the analysis of confocal Raman image of maize protoplasts. (D) Left panel: protochlorophyllide concentration map. Center panel: carotenoid concentration map. Right panel: Merged red and green color overlay, where the protochlorophyllide image is assigned to the red channel and carotenoid image is assigned to the green channel. Arrows highlight examples of plastid heterogeneity. (E) and (F). Two additional protoplasts. Image panels for E and F are the same as in D. Scale bars = 5 μm. (note: **Figure 3** is best viewed in color. Please refer to the online version of this chapter for the color version of **Figure 3**).

Synechocystis 6803 [48]; however, the spectral resolution of such a system is not sufficient to resolve different carotenoids.

Synechocystis 6803 has emerged as a model cyanobacterium due to the ease of genetic manipulation. Although *Synechocystis* 6803 cells are quite small (1.5–2 μm), Raman spectroscopic imaging can provide information about subcellular carotenoid localization. **Figure 4** shows the results of Raman spectroscopic imaging of wild-type *Synechocystis* 6803 cells. The carotenoid spectrum isolated in **Figure 4A** has ν_1 vibration appearing at 1515 cm^{-1} and ν_2 vibration at 1155 cm^{-1}, identifying that carotenoid most likely corresponds to beta-carotene, one of the major carotenoid species in *Synechocystis* 6803. The phycobilin spectrum peak is centered at ~3250 cm^{-1} (equivalent to 643.2 nm) and thus corresponds to phycocyanin, the primary pigment found in the antenna structure. The fluorescence emission of phycocyanin is ~645 nm. While subcellular details are somewhat limited given the small number of pixels in each cell, cell-to-cell differences in localization patterns are clearly evident. For example, in **Figure 4**, the carotenoids in the dividing cell on the left are concentrated into one small foci on each cell, whereas in the other, two cells have carotenoids localized more uniformly through the thylakoid membranes that house the light-harvesting complexes, similar to the phycocyanin.

http://dx.doi.org/10.5772/68101

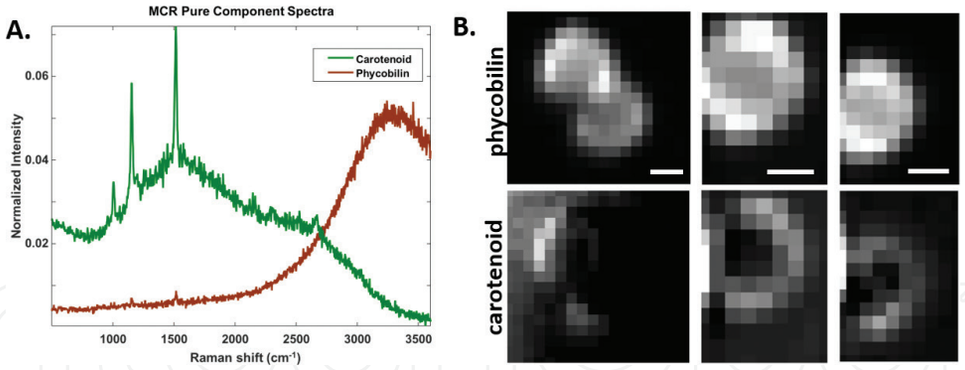

Figure 4. Results from confocal Raman-spectroscopic imaging of wild-type *Synechocystis* 6803 cells. (A) MCR identified pure component spectra. A fourth component consisting of a tail at ~3500 cm^{-1} was isolated as well and corresponds to chlorophyll. It was omitted for simplicity. (B) MCR concentration maps indicating carotenoid (bottom row) and phycobilin (top row) abundance for three different cells. Image intensities have been independently scaled between for maximum visibility; however, all intensity scales are within 20% of each other. A concentration map for the offset component is not shown. Scale bar = 1 μm.

Cell-to-cell heterogeneity and population dynamics are important to understand cyanobacterial adaptation to changes in the abiotic or biotic environment and could be addressed with Raman spectroscopic imaging in the future. It is also important to note that the images in **Figure 4** were collected under slightly less than diffraction-limited conditions. Improvements in spatial resolution are possible with a more optimal arrangement.

4. Conclusions

Localizing carotenoids in living cells and tissues is challenging due to the complex biological matrices of the living cells and intense sometimes colocated interfering fluorescence. Raman spectroscopic imaging coupled with multivariate curve resolution analysis provides the necessary spatial and chemical resolution to identify highly similar carotenoids even in the midst of highly overlapping, strong chlorophyll emission and complex backgrounds. Three examples were presented that highlight different advantages of the methodology for investigating photosynthetic organisms. Recent technological advances in detector speed and sensitivity will most likely catalyze future investigations of carotenoid biogenesis in single cells, including population dynamics and response to changing environmental conditions, by facilitating time-course studies that were previously prohibitive given the long scan times required for Raman spectroscopic imaging. These capabilities are anticipated to impact a variety of research areas including carbon partitioning and utilization, microbial ecology, and crop analytics.

Acknowledgements

The authors are grateful to the following people for their assistance with the research presented in this chapter: Anthony McDonald for assistance with the collection of Raman spectroscopic image data; Meghan Dailey for culturing the *Synechocystis* 6803; Stephen Anthony

for the current implementation of the MCR analysis software used to deconvolve spectral components; Howland Jones, Mark Van Benthem, David Melgaard, Mike Keenan, and David Haaland for original development of the MCR algorithm and software; Wim Vermaas, Arizona State University, for the gift of the purified carotenoid standards, Himadri Pakrasi, Washington University, St. Louis, for the gift of *Synechocystis sp*. PCC 6803; Qiang Hu for the gift of the *H. pluvialis*.

This research was primarily supported as part of the Photosynthetic Antenna Research Center (PARC), an Energy Frontier Research Center funded by the U.S. Department of Energy (DOE), Office of Science, Basic Energy Sciences (BES), under Award # DE-SC 0001035 (Maize protoplasts imaging, Synechocystis imaging, writing), by Sandia National Laboratories' Laboratory Directed Research and Development (LDRD) Program under Award # 141528 (*H. pluvialis* imaging), and by funding from the National Institutes of Health (GM081160) (to ETW) for research on carotenoids in maize protoplasts. Sandia National Laboratories is a multimission laboratory managed and operated by Sandia Corporation, a wholly owned subsidiary of Lockheed Martin Corporation, for the U.S. Department of Energy's National Nuclear Security Administration under contract DE-AC04-94AL85000.

Author details

Jerilyn A. Timlin[1]*, Aaron M. Collins[2], Thomas A. Beechem[1], Maria Shumskaya[3,5] and Eleanore T. Wurtzel[3,4]

*Address all correspondence to: jatimli@sandia.gov

1 Sandia National Laboratories, Albuquerque, NM, USA

2 Southern New Hampshire University, Manchester, NH, USA

3 Department of Biological Sciences, Lehman College, The City University of New York (CUNY), Bronx, New York, NY, USA

4 The Graduate School and University Center-CUNY, New York, NY, USA

5 Department of Biology, School of Natural Sciences, Kean University, Union, NJ, USA

References

[1] Frank HA, Cogdell RJ. Carotenoids in photosynthesis. Photochem Photobiol. 1996;**63**: 257–64. DOI: 10.1111/j.1751-1097.1996.tb03022.x.

[2] Demmig-Adams B, Adams Iii WW. The role of xanthophyll cycle carotenoids in the protection of photosynthesis. Trends Plant Sci. 1996;**1**:21–6. DOI: 10.1016/S1360-1385(96)80019-7.

[3] Bartley GE, Scolnik PA. Plant carotenoids: pigments for photoprotection, visual attraction, and human health. The Plant Cell. 1995;**7**:1027–38.

[4] Lewis IR, Edwards HGM, editors. Handbook of Raman Spectroscopy. New York: Marcel Dekker, Inc.; 2001.

[5] Vankeirsbilck T, Vercauteren A, Baeyens W, Van der Weken G, Verpoort F, Vergote G, et al. Applications of Raman spectroscopy in pharmaceutical analysis. TrAC Trends in Analytical Chemistry. 2002;**21**:869–77. DOI: 10.1016/S0165-9936(02)01208-6.

[6] Clegg IM, Everall NJ, King B, Melvin H, Norton C. On-line analysis using Raman spectroscopy for process control during the manufacture of titanium dioxide. Appl Spectrosc. 2001;**55**:1138–50. DOI: 10.1366/0003702011953388.

[7] Efremov EV, Ariese F, Gooijer C. Achievements in resonance Raman spectroscopy: review of a technique with a distinct analytical chemistry potential. Anal Chim Acta. 2008;**606**:119–34. DOI: 10.1016/j.aca.2007.11.006.

[8] Robert B. Resonance Raman spectroscopy. Photosynth Res. 2009;**101**:147–55. DOI: 10.1007/s11120-009-9440-4.

[9] Merlin JC. Resonance Raman spectroscopy of carotenoids and carotenoid-containing systems. Pure Appl Chem. 1985;**57**:785–92.

[10] Rimai L, Heyde ME, Gill D. Vibrational spectra of some carotenoids and related linear polyenes. Raman spectroscopic study. J Am Chem Soc. 1973;**95**:4493–501. DOI: 10.1021/ja00795a005.

[11] Gill D, Kilponen RG, Rimai L. Resonance Raman scattering of laser radiation by vibrational modes of carotenoid pigment molecules in intact plant tissues. Nature. 1970;**227**:743–4.

[12] Klein K, Gigler Alexander M, Aschenbrenner T, Monetti R, Bunk W, Jamitzky F, et al. Label-free live-cell imaging with confocal Raman microscopy. Biophys J. 2012;**102**:360–8. DOI: 10.1016/j.bpj.2011.12.027.

[13] Dieing T, Hollricher O, Toporski J, editors. Confocal Raman Microscopy: Springer-Verlag Berlin Heidelberg Springer; 2011.

[14] Morris HR, Hoyt CC, Miller P, Treado PJ. Liquid crystal tunable filter Raman chemical imaging. Appl Spectrosc. 1996;**50**:805–11.

[15] Timlin JA, Carden A, Morris MD. Chemical microstructure of cortical bone probed by Raman transects. Appl Spectrosc. 1999;**53**:1429–135.

[16] Christensen KA, Morris MD. Hyperspectral Raman microscopic imaging using Powell lens line illumination. Appl Spectrosc. 1998;**52**:1145–7.

[17] Schlucker S, Schaeberle MD, Huffman SW, Levin IW. Raman microspectroscopy: A comparison of point, line, and wide-field imaging methodologies. Anal Chem. 2003; **75**:4312–8.

[18] Kong L, Navas-Moreno M, Chan JW. Fast confocal Raman imaging using a 2-D multifocal array for parallel hyperspectral detection. Anal Chem. 2016;**88**:1281–5. DOI: 10.1021/acs.analchem.5b03707.

[19] Wu H, Volponi JV, Oliver AE, Parikh AN, Simmons BA, Singh S. *In vivo* lipidomics using single-cell Raman spectroscopy. Proc Natl Acad Sci. 2011;**108**:3809–14. DOI: 10.1073/pnas.1009043108.

[20] Schuster KC, Urlaub E, Gapes JR. Single-cell analysis of bacteria by Raman microscopy: spectral information on the chemical composition of cells and on the heterogeneity in a culture. J Microbiol Meth. 2000;**42**:29–38.

[21] Gierlinger N, Keplinger T, Harrington M. Imaging of plant cell walls by confocal Raman microscopy. Nat Protocols. 2012;**7**:1694–708. DOI: 10.1038/nprot.2012.092.

[22] Huang WE, Griffiths RI, Thompson IP, Bailey MJ, Whiteley AS. Raman microscopic analysis of single microbial cells. Anal Chem. 2004;**76**:4452–8. DOI: 10.1021/ac049753k.

[23] Huang WE, Stoecker K, Griffiths R, Newbold L, Daims H, Whiteley AS, et al. Raman-FISH: combining stable-isotope Raman spectroscopy and fluorescence in situ hybridization for the single cell analysis of identity and function. Environ Microbiol. 2007;**9**:1878–89. DOI: 10.1111/j.1462-2920.2007.01352.x.

[24] Matthäus C, Krafft C, Dietzek B, Brehm BR, Lorkowski S, Popp J. Noninvasive imaging of intracellular lipid metabolism in macrophages by Raman microscopy in combination with stable isotopic labeling. Anal Chem. 2012;**84**:8549–56. DOI: 10.1021/ac3012347.

[25] Pudney PDA, Gambelli L, Gidley MJ. Confocal Raman microspectroscopic study of the molecular status of carotenoids in tomato fruits and foods. Appl Spectrosc. 2011;**65**:127–34. DOI: 10.1366/10-06121.

[26] Zheng Y-T, Toyofuku M, Nomura N, Shigeto S. Correlation of carotenoid accumulation with aggregation and biofilm development in Rhodococcus sp. SD-74. Anal Chem. 2013;**85**:7295–301. DOI: 10.1021/ac401188f.

[27] Collins AM, Jones HDT, Han D, Hu Q, Beechem TE, Timlin JA. Carotenoid distribution in living cells of *Haematococcus pluvialis* (Chlorophyceae). PLoS One. 2011;**6**:e24302.

[28] Toomey MB, Collins AM, Frederiksen R, Cornwall MC, Timlin JA, Corbo JC. A complex carotenoid palette tunes avian colour vision. J Royal Soc Interf. 2015;**12**. DOI: 10.1098/rsif.2015.0563.

[29] Haaland DM, Jones HDT, Timlin JA. Experimental and Data Analytical Approaches to Automating Multivariate Curve Resolution in the Analysis of Hyperspectral Images. In: Ruckebusch C, editor. Resolving Spectral Mixtures. Data Handling in Science and Technology. 30. Amsterdam: Elsevier; 2016. pp. 381–406.

[30] Zhang J, O'Connor A, Turner II JF. Cosine histogram analysis for spectral image data classification. Appl Spectrosc. 2004;**58**:1318–24.

[31] Widjaja E, Crane N, Chen T-c, Morris MD, Ignelzi Jr MA, McCreadie BR. Band-target entropy minimization (BTEM) applied to hyperspectral Raman image data. Appl Spectrosc. 2003;**57**:1353–62.

[32] Felten J, Hall H, Jaumot J, Tauler R, de Juan A, Gorzsás A. Vibrational spectroscopic image analysis of biological material using multivariate curve resolution–alternating least squares (MCR-ALS). Nat Protocols. 2015;**10**:217–40. DOI: 10.1038/nprot.2015.008.

[33] de Juan A, Tauler R. Chemometrics applied to unravel multicomponent processes and mixtures: Revisiting latest trends in multivariate resolution. Anal Chim Acta. 2003;**500**:195–210. DOI: 10.1016/S0003-2670(03)00724-4.

[34] Schoonover JR, Marx R, Zhang SL. Multivariate curve resolution in the analysis of vibrational spectroscopy data files. Appl Spectrosc. 2003;**57**:154A–70A.

[35] Webster S, Batchelder DN, Smith DA. Submicron resolution measurement of stress in silicon by near-field Raman spectroscopy. Appl Phys Lett. 1998;**72**:1478–80. DOI: 10.1063/1.120598.

[36] Shumskaya M, Bradbury LMT, Monaco RR, Wurtzel ET. Plastid localization of the key carotenoid enzyme phytoene synthase is altered by isozyme, allelic variation, and activity. The Plant Cell. 2012;**24**:3725–41. DOI: 10.1105/tpc.112.104174.

[37] Anthony SM, Timlin JA. Removing cosmic spikes using a hyperspectral upper-bound spectrum method. Appl Spectrosc. 2016:0003702816668528. DOI: 10.1177/0003702816668528.

[38] Jones HDT, Haaland DM, Sinclair MB, Melgaard DK, Collins AM, Timlin JA. Preprocessing strategies to improve MCR analyses of hyperspectral images. J Chemomet Intell Lab Syst. 2012;**117**:149–58. DOI: 10.1016/j.chemolab.2012.01.011.

[39] Van Benthem MH, Keenan MR, inventors; Sandia Corporation, assignee. Fast combinatorial algorithm for the solution of linearly constrained least squares problems. US2008.

[40] Van Benthem MH, Keenan MR. Fast algorithm for the solution of large scale non-negativity constrained least squares problems. J Chemom. 2004;**18**:441–50.

[41] Ohlhausen JA, Keenan MR, Kotula PG, Peebles DE. Multivariate statistical analysis of time-of-flight secondary ion mass spectrometry images using AXSIA. Appl Surf Sci. 2004;**231-232**:230–4.

[42] Kotula PG, Keenan MR, Michael JR. Automated analysis of SEM X-Ray spectral images: a powerful new microanalysis tool. Microsc Microanal. 2003;**9**:1–17.

[43] Van Benthem MH, Keenan MR, Haaland DM. Application of equality constraints on variables during alternating least squares procedures. J Chemom. 2002;**16**:613–22.

[44] Schindelin J, Arganda-Carreras I, Frise E, Kaynig V, Longair M, Pietzsch T, et al. Fiji: an open-source platform for biological-image analysis. Nat Meth. 2012;**9**:676–82. DOI: 10.1038/nmeth.2019.

[45] Robertson DS, Bachmann MD, Anderson IC. Role of carotenoids in protecting chlorophyll from photodestruction—II. Studies on the effect of four modifiers of the albino cl1 mutant of maize. Photochem Photobiol. 1966;**5**:797–805. DOI: 10.1111/j.1751-1097.1966.tb05775.x.

[46] Ruban AV, Pascal A, Lee PJ, Robert B, Horton P. Molecular configuration of xanthophyll cycle carotenoids in photosystem II antenna complexes. J Biol Chem. 2002;**277**:42937–42. DOI: 10.1074/jbc.M207823200.

[47] Blankenship RE. Molecular Mechanisms of Photosynthesis: Wiley-Blackwell; Oxford 2013. 336 p.

[48] Vermaas WFJ, Timlin JA, Jones HDT, Sinclair MB, Nieman LT, Hamad S, et al. *In vivo* hyperspectral confocal fluorescence imaging to determine pigment localization and distribution in cyanobacterial cells. Proc Natl Acad Sci. 2008;**105**:4050–5.